American Mineralogist, Volume 83, pages 1054–1066, 1998

Molecular cluster models of aluminum oxide and aluminum hydroxide surfaces

J.D. KUBICKI[1,*] AND S.E. APITZ[2]

[1]Computer Sciences Corporation, 4045 Hancock Street, San Diego, California 92110-5164
[2]Remediation Research Laboratory, Chemistry and Biochemistry Branch, Space and Naval Warfare Systems Center D361, San Diego, California 92152-6325

ABSTRACT

Ab initio, molecular orbital calculations for two different Hartree-Fock basis levels were performed on clusters in the system Al-O-H, and tested by comparing derived vibrational frequencies to the measured values for aluminum oxides and aluminum oxyhydroxide minerals. Models were chosen to reflect surface groups that may be present on aluminous minerals such as α-Al_2O_3 (corundum) and $Al(OH)_3$ (gibbsite). Protonation and deprotonation reactions on bridging and terminal oxygen or hydroxyl sites were modeled to investigate the effects of solution *pH* on the structure of surface groups. Relative deprotonation energies, including solvation effects, were calculated for each site using the self-consistent isodensity polarized continuum model of Keith and Frisch (1994), and then used to predict the order in which each particular surface group protonates.

INTRODUCTION

Surfaces of aluminum oxide and oxyhydroxide minerals have been investigated for many years (see Boehm 1966 for a review). Models of the surface groups present on these minerals have been derived from interpretations of surface titrations (e.g., Stumm and Morgan 1981; Schindler and Stumm 1987) and infrared band assignments (e.g., Tsyganenko and Filimonov 1973; Morterra et al. 1976; Boehm and Knözinger 1983; Koretsky et al. 1997). These models have been used to explain adsorption and dissolution reactions of mineral surfaces in soils and sediments (e.g., Davis and Leckie 1978; Furrer and Stumm 1986; Schindler and Stumm 1987). Extrapolation of these models based on oxides for use as end-member components in feldspars (Parks 1967) has made the surface protonation concepts proposed by Stumm and coworkers (Hochella and White 1990 and references therein) the most common view of mineral surfaces in geochemistry.

Models of speciation on mineral surfaces are often oversimplified. Numerous oxygen or hydroxyl sites exist on mineral surfaces; and the pK_a of each type may be affected by the crystal face that it occurs on, and position on terrace, edge, or kink sites (Bleam et al. 1993; Rustad et al. 1996). Bulk pK_a's for minerals lump all these effects into a single value and do not account for variations in reactivity at different surface sites. To understand mineral dissolution reactions, the concept of reactive surface sites is an important one. For example, mineral dissolution is commonly described as proportional to mineral surface area (Lasaga 1981); but long-term dissolution can, at times, increase the mineral surface area and decrease the dissolution rate (Stillings and Brantley 1995). One explanation of this phenomenon is that higher energy sites are consumed first, leading to the formation of micropores or etch pits (Holdren and Berner 1979; Berner and Holdren 1979; Berner et al. 1980; Hochella and Banfield 1995) that increase surface area. The loss of higher energy surface sites also has been used to explain $[H_4SiO_4]$ concentration profiles in sediments where aqueous silica is high initially and decreases to a constant value at depth (Van Cappellen and Qiu 1995). As lower energy sites come to dominate the mineral surface, dissolution slows because the ΔG of reaction decreases (Burch et al. 1993).

One purpose of this paper is to help differentiate among various pK_a's associated with individual surface sites that may contribute to overall pK_a's measured for minerals. In this manner, it may be possible to derive relative speciations of each site as a function of *pH* for each mineral surface (e.g., Sverjensky and Sahai 1996). Detailed mineral surface speciation would be useful in deciphering the mechanisms of mineral dissolution.

Another purpose of this study is to build a basis for modeling sorption reactions on aluminum oxide and oxyhydroxide surfaces. Adsorption of metals and organic ligands to mineral surfaces is an important topic in environmental geochemistry because these reactions affect the transport and fate of contaminants in soils, aquifers, and sediments (Knezovich et al. 1987; Rebhun et al. 1992). Molecular modeling of adsorption reactions first requires theoretical models of the mineral surfaces themselves. Earlier quantum mechanical studies of aluminate surfaces have been carried out (Kawakami et al. 1984; Kawakami and Yoshida 1985; Keyes and Watters 1989), but recent software and hardware developments allow substantial improvements to this previous work. Specifi-

* E-mail: kubicki@nosc.mil

0003–004X/98/0910–1054$05.00

cally, vibrational spectroscopic properties (Frisch et al. 1995) can be calculated and compared with observed values, and the long-range effects of solvation may now be included.

Calculational details

Calculations were performed with Gaussian 94 (Frisch et al. 1995). Molecular structures were determined by searching the molecular potential energy surfaces for a minimum with respect to all atomic coordinates using a HF/3-21G** basis set (Foresman and Frisch 1993). The chosen basis set is relatively small to locate stable structures efficiently, but it reproduces bond distances and angles in aluminosilicates (Kubicki et al. 1996). Location of minimum energy structures were verified by performing force constant analyses on the system to ensure that no imaginary frequencies (i.e., unstable vibrational modes) were present for a given configuration. Frequencies obtained in the force constant analyses were scaled by 0.89 to account for anharmonicity, basis set limitations, and neglect of electron correlation effects (Pople et al. 1981) before comparison with experimental values. Molecular energy calculations were also carried out with a HF/6-311+G** basis set (Foresman and Frisch 1993) in the HF/3-21G** energy-minimized structures. Corrections for zero-point energy (ZPE) were taken from the HF/3-21G** force constant analyses. This procedure has been shown to provide fairly accurate estimates of gas-phase proton affinities (Kubicki et al. 1997).

Corrections for solvation energies were made with self-consistent isodensity polarized continuum model (SCIPCM) calculations (Keith and Frisch 1994). The clusters were surrounded by a dielectric continuum (ϵ = 78.54 for water at standard T and P) without further energy minimization. The electron density contour cutoff was selected as 0.001 electrons (Wong et al. 1995). Protonation and deprotonation energies were then calculated from reactions such as

$$Al_2(OH)_6(OH_2)_4 + H_3O^+ \cdot 8(H_2O) \rightarrow [Al_2(OH)_5(OH_2)_5]^+ + H_2O \cdot 8(H_2O) \quad (1)$$

and

$$Al_2(OH)_6(OH_2)_4 + OH^- \cdot 8(H_2O) \rightarrow [Al_2(OH)_7(OH_2)_3]^- + H_2O \cdot 8(H_2O) \quad (2)$$

where each cluster is in a dielectric continuum.

The neutral model clusters $Al_2O_3(H_2O)_6$, $Al_2O(OH)_4(H_2O)_4$, $Al_2(OH)_6(H_2O)_4$, $[(H_2O)_3(OH)_2Al(OH)Al(OH)_3]$, $Al_2(OH)_6$, and $Al_3O_{13}H_{17}$ were chosen to model surface reactions on α-Al_2O_3 (corundum), $Al(OH)_3$ (gibbsite), γ-Al_2O_3 and a hypothetical tetrahedral $Al(OH)_3$ phase. The cluster $Al_3O_{13}H_{17}$ was also modeled to obtain a structure with an O atom bonded to three Al atoms. However, no stable potential energy minimum could be found for this cluster. The clusters listed above are electrostatically neutral, representing a mineral surface near the point of zero charge (PZC). Protonation and deprotonation of O sites in each of these model clusters was performed, followed by two types of structural relaxation. The first type allowed only movement of the O and H atoms in the group undergoing protonation or deprotonation. This method approximates possible restrictions imposed by lattice constraints on a real mineral surface. The second type allowed for full relaxation of the cluster to obtain a new structure that could provide vibrational frequencies of the protonated or deprotonated group. In this manner, upper and lower bounds were predicted for the effects of lattice constraints on the proton affinities of our calculated model clusters.

For each of the model mineral clusters in this study, corundum, gibbsite, γ-Al_2O_3, and tetrahedral $Al(OH)_3$ (Carroll-Webb and Walther 1988; Brady and Walther 1989; Blum and Lasaga 1991; Oxburgh et al. 1994), we present molecular structures of the potential energy minima. Structural changes that occur with protonation and deprotonation of various O sites within the clusters are also discussed. The validity of these molecular cluster calculations as representations of mineral surface structures is analyzed by comparing the O-H vibrational frequencies calculated for the clusters to those measured on mineral surfaces. Agreement between model and experimental frequencies is good, so we attempt to relate the model structural changes accompanying protonation and deprotonation reactions to mineral surface structure and dissolution. The link between model structures and mineral surfaces is made via calculation (Eqs. 1 and 2) of the relative proton affinities of each site. This may be used to suggest possible mineral surface reactions as a function of solution *pH*.

Results and discussion

Structures

Corundum model clusters. Figure 1a shows a partially optimized structure based on a starting configuration of $Al_2O_3(H_2O)_6$ with face-sharing octahedra. The O-H distances in the H_2O molecules were constrained to 0.94 Å (an average value calculated with this basis set for O-H bonds in aluminates) to prevent proton transfer to the bridging O atoms. The Al-O bond distances in this molecule are 1.83 for the bridging bonds and 1.99 Å for the Al-OH_2 bonds. These values compare favorably with bond lengths of 1.86 and 1.97 Å in corundum (Wyckoff 1978). However, in our model molecule, the bridging Al-O bonds are the shorter bonds compared to the Al-OH_2 bonds; whereas in corundum, the Al-O bonds to the shared face are longer.

Deprotonation of one terminal Al-(OH_2) group was modeled in two steps. First, a proton was removed from the Al-(OH_2) group followed by relaxation of the O1-H1 bond length in the terminal OH group. Second, another energy minimization was performed with only the O-H bond lengths in the H_2O molecules constrained. This second step results in the configuration shown in Figure 1b. These two steps represent deprotonation of a surface Al-

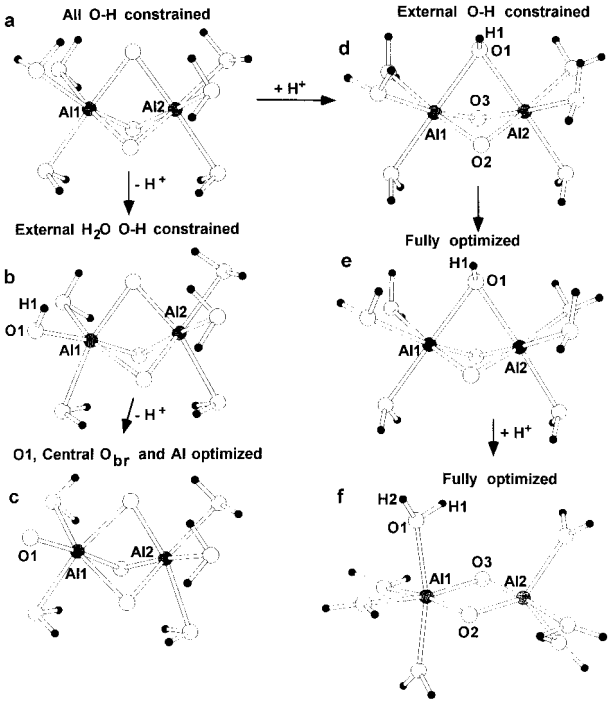

FIGURE 1. Corundum I model clusters: (**a**) neutral $Al_2O_3(H_2O)_6$, (**b**) deprotonated terminal Al-OH_2, (**c**) deprotonated terminal Al-OH, (**d**) protonated bridging O with external O-H bond lengths constrained, (**e**) fully relaxed protonated bridging O structure, and (**f**) unconstrained, energy minimized structure after protonation of Al-(OH)-Al group. All molecular structures drawn with the program Atoms (Dowty 1995). Open circles = O; gray circles = Al; black dots = H atoms.

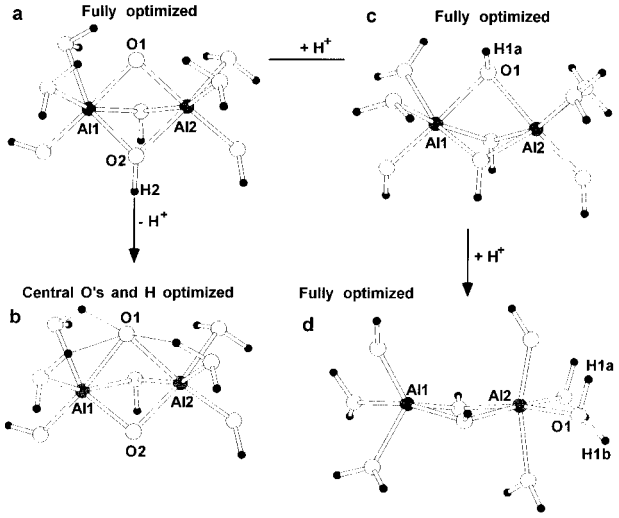

FIGURE 2. Corundum II clusters: (**a**) neutral $Al_2O(OH)_4(H_2O)_4$, (**b**) deprotonated Al-(OH)-Al group after relaxation of bridging O atoms and OH group only, (**c**) energy minimum after protonation of bridging O in Al-O-Al, and (**d**) fully relaxed structure after protonation of Al-(OH)-Al linkage. See Figure 1 caption for symbols.

(OH_2) group in Al_2O_3 with strong lattice constraints in the first case and with surface structure relaxation in the second case. The most significant structural change with deprotonation is that the Al1-O_{br} bond increases to 2.11 Å and the corresponding Al2-O_{br} bond decreases to 1.75 Å (Fig. 1b). Deprotonating the Al1-O1H1 group with relaxation of the O1, Al, and O_{br} atoms to form the complex in Figure 1c leads to a terminal Al-O1 bond of 1.68 Å and an Al1-O_{br} bond of 2.19 Å. Thus, if the Al1 atom were on a mineral surface, the linkage of this surface atom to the bulk mineral would be lengthened with the formation of Al-O^-.

Similar step-wise structural re-optimizations are shown in Figures 1d and 1e for the protonation of a bridging O on an Al_2O_3 surface. First, the position of H1 was optimized. Then, the external O-H distances were constrained and the remainder of the structure relaxed (Fig. 1d). The molecule was then fully optimized (Fig. 1e). In this case, both the Al-O_{br} distances to the protonated O are lengthened to an average value of 1.97 Å. This lengthening implies that less energy will be required to cleave the Al-O-Al linkage once the bridging O has been protonated. In fact, a second protonation of the bridging O (Fig. 1f) breaks the linkage and forms a dimer with one octahedral and one pentahedral Al^{3+}. This dimer is 613 kJ/mol lower in energy than the constrained Al-(OH_2)-Al form of the complex. If water were present, the pentahedral Al^{3+} should not re-hydrate because

$$Al_2O_2\text{-}(H_2O)_7 + H_2O \rightarrow Al_2O_2\text{-}(H_2O)_8 \qquad (3)$$

has a calculated ΔE of +30 kJ/mol with SCIPCM HF/6-311+G** calculations. In addition, the ΔS for the water adsorption reaction would be negative making the ΔG of reaction 3 even more positive. On a mineral surface, one of the other bridging O atoms (O2 or O3) would protonate before the second protonation of O1. Thus, a $^{[4]}$O atom with two Al-O and two O-H bonds does not appear to be an energetically favorable structure. Addition of a second proton to an existing Al-(OH)-Al linkage should break the linkage. Such a rupture would be an important step in the dissolution process. Because no energy barrier exists to breaking the Al-(OH_2)-Al linkage once it is formed, the activation energy of dissolution would depend on the energy barrier for a proton transfer from H_3O^+ to an Al-(OH)-Al group.

The $Al_2O_3(H_2O)_6$ cluster (Fig. 1a) is +436 kJ/mol higher in energy than the fully optimized configuration, $Al_2O(OH)_4(H_2O)_4$ in Figure 2a. This lower energy configuration forms during full energy minimization as the result of proton transfers from terminal H_2O groups to two of the bridging O atoms. In the fully optimized configuration, the average Al-O_{br} and Al-OH_{br} distances are 1.83 and 1.92 Å, respectively. These values are reasonably close to those observed in corundum. The Al-OH_2 distances in Figure 2a are also close to normal octahedral values for Al^{3+} (2.00 Å), but the Al-OH distance for the non-bridging O atoms is only 1.75 Å, close to tetrahedral values for Al^{3+} (Shannon and Prewitt 1969).

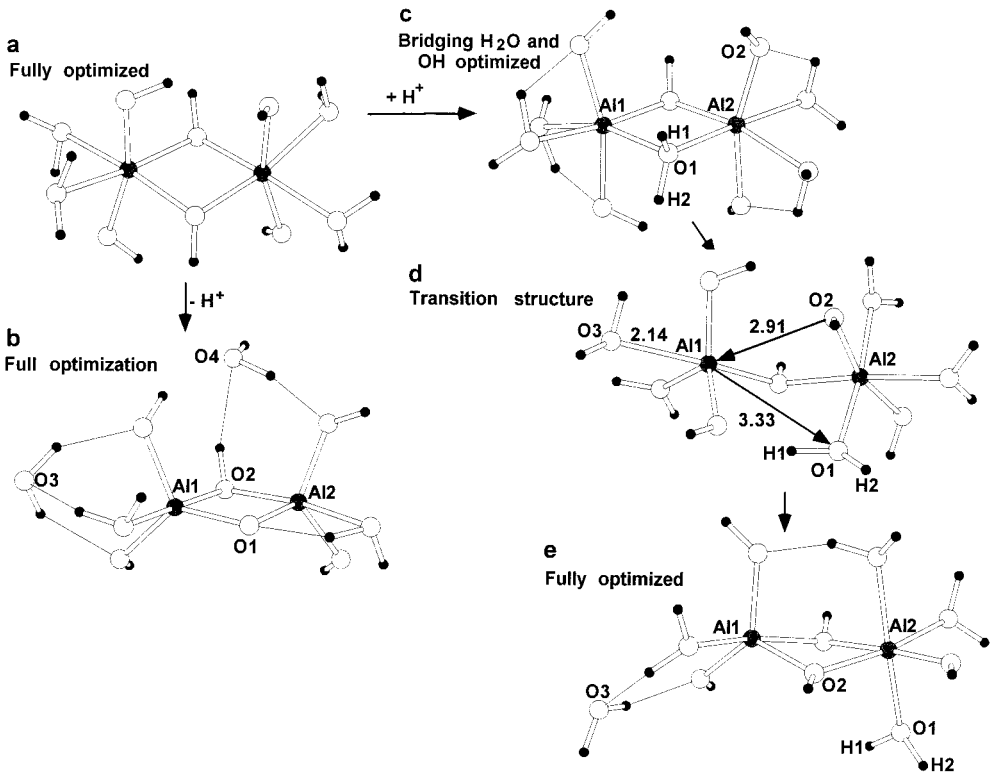

FIGURE 3. Bridging protonation and deprotonation reactions for model gibbsite cluster: (**a**) neutral $Al_2(OH)_6(H_2O)_4$, (**b**) fully optimized structure after deprotonation of bridging O, (**c**) structure after protonation of Al-(OH)-Al group with only bridging OH and OH_2 groups relaxed, (**d**) configuration along the reaction path from two [6]Al atoms to the [5]Al-[6]Al dimer, and (**e**) the energy minimized structure after protonation of an Al-(OH)-Al group. See Figure 1 caption for symbols.

Deprotonation of a bridging OH group in $Al_2O(OH)_4(H_2O)_4$ (O2-H2 in Fig. 2a) to form $Al_2O_2(OH)_3(H_2O)_4$ (Fig. 2b) shortens one Al-O-Al linkage from 1.83 to 1.79 Å and lengthens the other Al-O-Al linkage to 1.95 Å. The Al-OH-Al bonds now average 2.03 Å; and hence, these bonds will be much weaker in the deprotonated complex than in the neutral complex.

Protonation of O1 in Figure 2a to form $Al_2(OH)_5(H_2O)_4$ (Fig. 2c) lengthens the Al-(O1H1a)-Al bridge to 1.90 Å from 1.83 Å. Otherwise, this first protonation does not alter the structures (Figs. 2a and 2c) dramatically. A second protonation of O1, however, changes the character of the cluster. Constrained minimization ends with a breakage of the Al-(O1H1a)-Al linkage present in Figure 2c and formation of pentacoordinate Al atoms. Unconstrained minimization predicts a structure (Fig. 2d) with one pentacoordinate and one octahedral Al atom linked by two Al-(OH)-Al linkages instead of the three found in Figure 2c. As discussed above for the Al_2O_2-$(H_2O)_7$ complex, re-hydration is energetically unfavorable (although only by +8 kJ/mol in this case) for the reaction

$$Al_2(OH)_4\text{-}(H_2O)_5 + H_2O \rightarrow Al_2(OH)_4\text{-}(H_2O)_6. \quad (4)$$

Gibbsite clusters. The $Al_2(OH)_6(H_2O)_4$ molecular cluster model (Fig. 3a) reproduces experimental bond lengths and angles found in gibbsite (Saalfeld and Wedde 1974). For instance, experimental bridging Al-(OH) bond lengths range from 1.88 to 1.92 Å and the average theoretical value is 1.89 Å. Within the Al-(OH)-Al-(OH) ring, experimental OAlO and AlOAl angles are approximately 80 and 100°, respectively, compared with 84 and 96° in the model dimer. One important discrepancy is in the O-H bond lengths for the bridging hydroxyl groups. Experiment gives 0.84 to 0.88 Å (Saalfeld and Wedde 1974), but the theoretical values are 0.94 Å. The experimental values are short compared to normal O-H bond distances of approximately 0.96 Å. Our values are also close to those obtained by Xiao and Lasaga (unpublished manuscript) with Hartree-Fock and density functional calculations on the same cluster. Theory may actually provide a more accurate estimate of O-H bond length in this instance due to the difficulties in determining H positions in minerals from crystallography.

Both protonation and deprotonation of one bridging (OH) group in this cluster drive Al coordination changes. In the case of deprotonation (Fig. 3b), the bridging Al-O bond is shortened significantly (from 1.89 to 1.74 Å) such that both Al atoms convert to distorted pentacoordinate species. Protonation of the bridging OH group causes a rupture of the original Al-(OH_2)-Al linkage (Fig. 3c). However, during energy minimization of the structure in Figure 3c, the Al2-(O2H) group in Figure 3d re-attaches

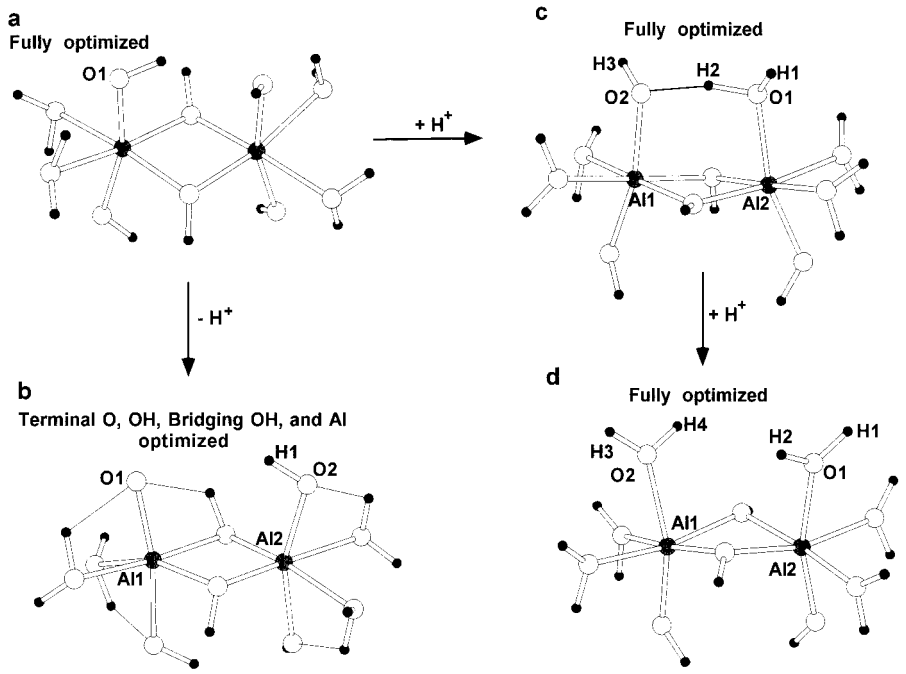

FIGURE 4. Terminal protonation and deprotonation reactions for model gibbsite cluster: (**a**) neutral $Al_2(OH)_6(H_2O)_4$, (**b**) partially optimized cluster after deprotonation of a terminal Al-OH group, (**c**) energy minimized cluster after protonation of terminal Al-OH, and (**d**) fully relaxed structure after protonation of a second terminal Al-OH group to form vicinal Al-OH_2^+ groups. See Figure 1 caption for symbols.

to the pentacoordinate Al1. At the same time, one of the terminal H_2O groups on the pentacoordinate Al leaves, resulting in a dimer between a pentacoordinate Al and an octahedral Al (Fig. 3e). The pentacoordinate Al in this $^{[5]}$Al-$^{[6]}$Al dimer appears to be stable because a water molecule is present nearby but does not bond to Al1 (Fig. 3e). Furthermore, the calculated energy of the complex in Figure 3e is −39 kJ/mol lower than that calculated for the isocompositional dimer $Al_2(OH)_5$-5(H_2O) composed of two octahedral Al^{3+} ions (Kubicki et al., unpublished manuscript). If this model is accurate, it may be possible to detect fivefold-coordinated ^{27}Al on high-surface area gibbsite crystals reacted in acidic solutions.

Proton reactions at the terminal Al-(OH) sites in the gibbsite model have much less effect on the molecular structure. After deprotonation of the O1 site in Figure 4a to form $Al_2O(OH)_5$-4(H_2O) (Fig. 4b), structural relaxation of the terminal Al-O1, Al-(OH), bridging Al-(OH), and Al positions results in an Al-O1 bond of 1.68 Å. Shortening this terminal bond and giving the complex a negative charge causes the Al1-$(OH)_{br}$ bonds to stretch to 1.95 Å compared to the original 1.88 Å in the neutral gibbsite model complex (Fig. 4a). As predicted for the corundum model, deprotonation of a surface Al-(OH) results in a weaker linkage of the Al atom involved in the deprotonation to the bulk mineral.

Sequential protonations of the terminal Al-(OH) groups in Figure 4a results in the structures shown in Figures 4c and 4d. Formation of the first Al-$(OH_2)^+$ group increases the bond length from 1.79 to 1.92 Å. The bridging Al-(OH) bond lengths on Al2 decrease slightly from 1.88 to 1.85 Å, thereby strengthening the linkage between the surface Al atom and the remainder of the cluster. Notably, hydrogen bonding between the terminal Al-$(OH_2)^+$ and Al-(OH) groups (Fig. 4c) is strong with a O1-H2 bond length of 1.03 Å and a H2—O2 distance of 1.43 Å. Protonation of the second terminal Al-(OH) group forms a pair of vicinal Al-$(OH_2)^+$ groups (Fig. 4d). Terminal Al-$(OH_2)^+$ bonds are stretched to 1.98 Å in this complex, but the bridging Al-(OH) bonds do not decrease further and return to values near those predicted for the neutral complex (i.e., 1.87 Å). Hydrogen bonding between the terminal Al-$(OH_2)^+$ groups is significantly reduced in this cluster as compared to Figure 4c.

γ-Al_2O_3. Figure 5a represents a component of γ-Al_2O_3 with octahedral and tetrahedral Al atoms linked by an OH group. The protonation state of each O atom in this complex has a greater effect on each Al-O bond length than the coordination state of the Al atom. For instance, Al-OH bonds on the octahedral Al average 1.78 Å compared with 1.99 Å for Al-OH_2 bonds in the octahedron and 1.73 Å for Al-OH bonds in the tetrahedron. As discussed above, protonation/deprotonation reactions can influence Al-coordination. Deprotonation of either a $^{[6]}$Al-OH_2 terminal group (Fig. 5b) or the $^{[6]}$Al-OH-$^{[4]}$Al bridging group (Fig. 5c) results in a decrease in coordination for the octahedral Al. In the first case, a $^{[4]}$Al is generated as the two remaining H_2O groups exit the coordination sphere

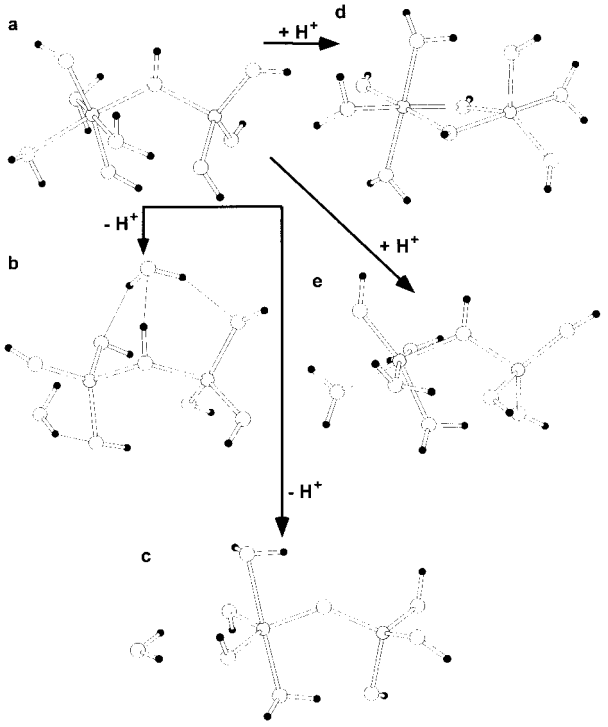

FIGURE 5. Fully optimized models of protonation and deprotonation in (**a**) neutral $[(H_2O)_3(OH)_2Al(OH)Al(OH)_3]$ with $^{[6]}Al$ and $^{[4]}Al$, (**b**) $^{[4]}Al$-$^{[4]}Al$ dimer after deprotonation of terminal Al-OH_2 group, (**c**) $^{[5]\text{ or }[4]}Al$ dimer after deprotonation of bridging Al-(OH)-Al, (**d**) protonated terminal $^{[4]}Al$-OH, and (**e**) protonated terminal $^{[6]}Al$-OH. See Figure 1 caption for symbols.

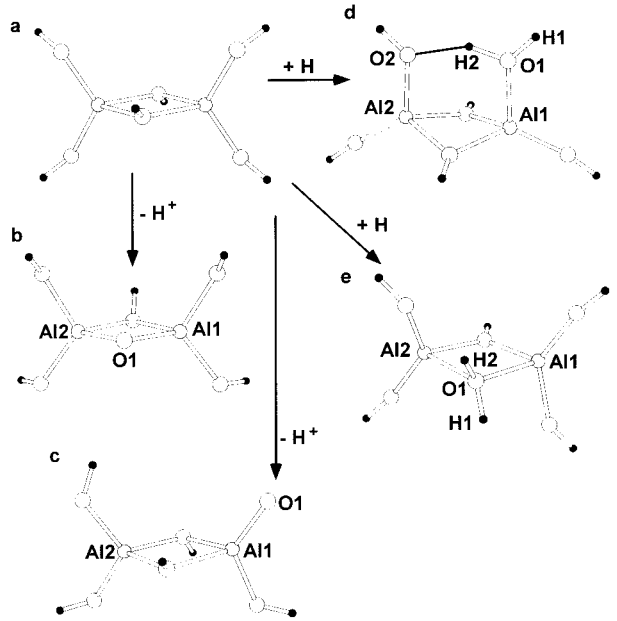

FIGURE 6. Fully optimized models of hypothetical tetrahedral $Al(OH)_3$: (**a**) $Al_2(OH)_6$, (**b**) deprotonation of bridging Al-(OH)-Al, (**c**) deprotonation of terminal Al-OH, (**d**) protonation of terminal Al-OH, and (**e**) protonation of bridging Al-(OH)-Al. See Figure 1 caption for symbols.

and hydrate the complex. This reaction mirrors the coordination change that occurs for Al^{3+} in aqueous solution as four Al-(OH) bonds are formed around the cation (Sykes et al. 1997). In the second case (Fig. 5c), deprotonation of the bridging OH group results in a $^{[5]}Al$ bonded to the original $^{[4]}Al$. This reaction is also predicted to occur in aqueous solution as three protons are removed from $Al^{3+}\cdot 6(H_2O)$ to form $Al(OH)_3$ (Sykes et al. 1997). Thus, both of these deprotonation reactions could be preparing surface $^{[6]}Al$ for solvation as tetrahedral $[Al(OH)_4]^-$.

Protonation of a terminal $^{[4]}Al$-OH group has the opposite effect. In Figure 5d, the tetrahedral Al converts to a pentacoordinate species and one of the remaining $^{[4]}Al$-OH groups bonds to the octahedral Al to form a second Al-(OH)-Al bridge. Adding a proton to a $^{[6]}Al$-OH group leads to the structure pictured in Figure 5e. Here, protonation decreases the $^{[6]}Al$-$(OH)_{br}$ distance from 1.89 to 1.86 Å. Both of these reactions on a mineral surface would tend to stabilize the Al atom on the surface rather enhance dissolution (Furrer and Stumm 1986; Wieland et al. 1988). Consequently, protonation of the bridging O is likely to be the mechanism that is a rate controlling step in the H^+ enhanced dissolution process rather than protonation of terminal Al-(OH) groups.

Tetrahedral $Al_2(OH)_6$. Surface titration results for feldspars are sometimes interpreted in terms of the surface chemistry of silica and a hypothetical aluminum hydroxide containing only $^{[4]}Al$ (Carroll-Webb and Walther 1988; Brady and Walther 1989; Blum and Lasaga 1991; Oxburgh et al. 1994). A hypothetical construct of such a surface cluster is generated (Fig. 6) solely for comparing theoretical proton affinities among different Al-hydroxide species. We do note, however, that no coordination changes or linkage breaks are generated by protonation or deprotonation of any hydroxide group. Furthermore, each of the configurations in Figure 6 are dynamically stable as evidenced by force constant analyses of these minimum energy structures. Hence, these represent possible molecular structures either on mineral surfaces or in aqueous solutions.

OH Frequencies

OH stretching vibrations in the terminal H_2O groups have a range of about 600 cm^{-1} (Fig. 7a) due to the variety of hydrogen bond strengths in the optimized structures of these clusters. This large range is consistent with the broad bands observed between 3000 and 3800 cm^{-1} for waters of hydration on mineral surfaces (Boehm 1966). The broad nature of this band makes it of limited utility for determining structures. However, ν(OH) frequencies can be correlated with O-H bond lengths (Novak 1974) and O-O distances in organic crystals (Nakamoto et al. 1955) and hydrogen bond lengths in tetrahedral aluminosilicate molecules (Kubicki et al. 1993) to give a range and distribution of these parameters from observed infrared bands. Figure 7a shows that the correlation is

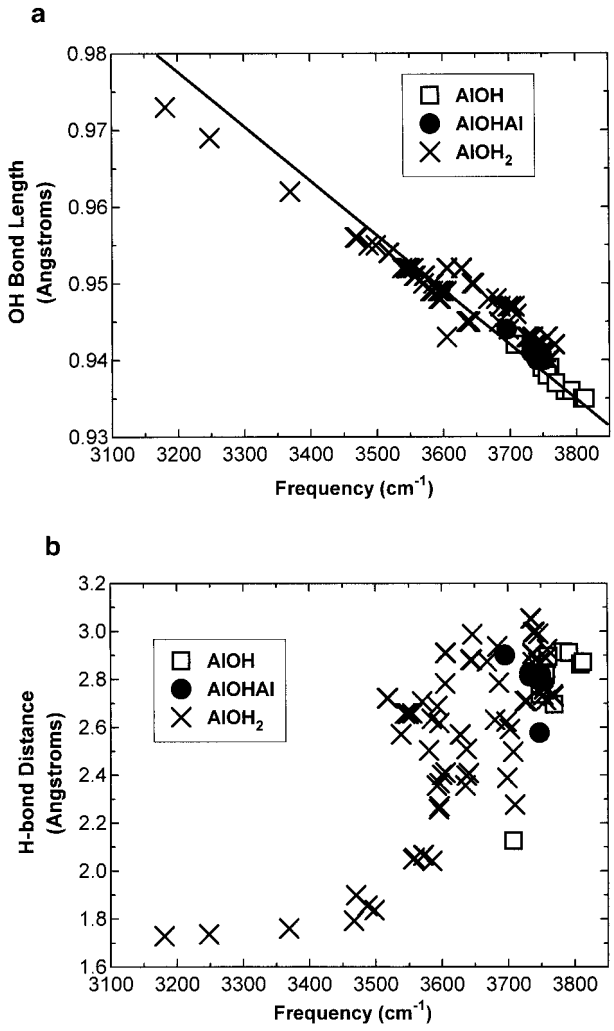

FIGURE 7. (**a**) Plot of O-H bond lengths vs. frequencies calculated in this study results in a strong linear correlation of these parameters as discussed in Novak (1974). (**b**) Theoretical hydrogen bond distances vs. calculated frequencies for the ν(OH) stretching modes of fully optimized molecules in this study does not show a linear relationship above 3500 cm^{-1}. A linear trend exists below 3500 cm^{-1}, but the slope is so shallow that it is not possible to accurately predict hydrogen bond distances based on ν(OH) frequencies.

strong (R^2 = 0.966) between O-H bond lengths and calculated ν(OH) stretching frequencies over the range of O-H bond lengths obtained for these aluminate molecules. The hydrogen bond distance correlation with frequency is weak for the octahedral Al species in the range 3500 to 3800 cm^{-1}, but a more linear trend may be defined below 3500 cm^{-1}. The results follow a similar trend to that observed by Nakamoto et al. (1955) for O-O distances vs. infrared frequencies. These trends are not dependent on the type of OH group (either terminal Al-OH, bridging Al-OH-Al, or Al-OH_2) involved in the ν(OH) stretch. We conclude that it is possible to use Figure 7a to predict the range of O-H bond lengths in phases with octahedral Al based on ν(OH) stretching frequencies. Unfortunately, the slope of hydrogen bond distances with frequency in Figure 7b does not allow prediction of these bond lengths from measured frequencies.

Corundum. Examination of the fully optimized corundum model, $Al_2O(OH)_4(H_2O)_4$, in Figure 2a reveals three types of OH groups: a bridging OH group bonded to two Al atoms, a terminal OH group bonded to one Al atom, and terminal H_2O groups. What we term octahedral bridging and terminal OH groups were designated IIb and Ib, respectively, by Knözinger and Ratnasamy (1978), but we prefer the former terminology as more descriptive. Table 1 contains the predicted OH stretching frequencies, ν(OH), from our model calculations and the range of values assigned for these species (Knözinger and Ratnasamy 1978). The agreement between the theoretical and experimental values is perhaps fortuitously close. At this level of theory, and with a molecular cluster approximation for the mineral surface, reproduction of measured frequencies is not expected to be exact (Kubicki et al. 1993). However, it is significant that the calculations reproduce the 50 cm^{-1} relative shift between the bridging and terminal hydroxyl groups. Relative frequency shifts are expected to be more reliable with this calculational methodology (Kubicki et al. 1993; Kubicki and Sykes 1993; Sykes and Kubicki 1996). The accurate reproduction of experimental frequencies suggests that the model cluster structures are not too different from the mineral surfaces; otherwise, the frequency agreement would be improbable. Furthermore, calculated proton affinities are also likely to be fairly reliable estimates for aluminol surface groups because ν(OH) frequencies correlate with acidities (Datka et al. 1988; Gil et al. 1994; Hunger et al. 1996).

Protonation of the bridging O to form $[Al_2(OH)_5(H_2O)_4]^+$ raises the bridging hydroxyl frequencies by about 10 cm^{-1}, but the terminal hydroxyl frequencies increase by approximately 40 cm^{-1} (Table 1). The excess positive charge has the effect of slightly shortening these O-H bonds and inducing the frequency increase. This prediction could be tested by collecting infrared spectra of the corundum surface after reaction with solutions of decreasing *pH*. To our knowledge, such a study has not been conducted on corundum.

Gibbsite. In the neutral gibbsite model complex (Fig. 4a), there are three types of OH groups: bridging OH, terminal OH, and terminal OH_2. As for the corundum model, ν(OH) of the bridging OH groups (Table 1) are in good agreement with experimental assignments (Boehm and Knözinger 1983). However, the calculated frequency range of the terminal or isolated Al-(OH) groups is approximately 30 cm^{-1} below that of the corresponding experimental values (Boehm and Knözinger 1983). The lower theoretical values could be due to weak hydrogen bonding between the Al-(OH) groups and the Al-(OH_2) groups used to terminate the model cluster. Although no H atom in an Al-(OH) group in this molecule is <2.1 Å from the next nearest O, several of the O atoms are 1.8 Å from neighbor H atoms in Al-(OH_2) groups. The com-

TABLE 1. Hydroxyl frequencies for molecular clusters

		Model	Calc. ν(OH) cm^{-1}	Expt. ν(OH) cm^{-1}
Corundum I model	$H^+Al_2O_3$-6(H_2O)	$^{[6]}$Al(OH)$^{[6]}$Al	3720	3740–3745(IIb)
Bridging Protonation		Al-OH_2	3140–3767	
Corundum II model	$[Al_2O(OH)_4(H_2O)_4]$	$^{[6]}$Al(OH)$^{[6]}$Al	3732–3742	3740–3745(IIb)
		$^{[6]}$Al-OH	3784–3792	3785–3800(Ib)
		Al-OH_2	3182–3746	
Bridging Protonation	$[Al_2(OH)_5(H_2O)_4]^+$	$^{[6]}$Al(OH)$^{[6]}$Al	3740–3750	3740–3745(IIb)
		$^{[6]}$Al-OH	3823–3830	3785–3800(Ib)
		Al-OH_2	3587–3790	
Gibbsite model	$[Al_2(OH)_6(H_2O)_4]$	$^{[6]}$Al(OH)$^{[6]}$Al	3747–3749	3740–3745(IIb)
		$^{[6]}$Al-OH	3747–3770	3785–3800(Ib)
		Al-OH_2	3370–3759	
Terminal Protonation	$[Al_2(OH)_5(H_2O)_5]^+$	$^{[6]}$Al(OH)$^{[6]}$Al	3730–3803	3740–3745(IIb)
		$^{[6]}$Al-OH	3758–3792	3785–3800(Ib)
		Al-OH_2	2207–3790	
	$[Al_2(OH)_4(H_2O)_6]^{2+}$	$^{[6]}$Al(OH)$^{[6]}$Al	3750–3751	3740–3745(IIb)
		$^{[6]}$Al-OH	3809–3813	3785–3800(Ib)
		Al-OH_2	3572–3757	
Bridging Deprotonation	$[Al_2O(OH)_5(H_2O)_4]^-$	$^{[5]}$Al(OH)$^{[5]}$Al	3668	3740–3745(IIb)
		$^{[5]}$Al-OH	3711–3774	3785–3800(Ib)
		Al-OH_2	3305–3742	
Bridging Protonation	$H^+[Al_2(OH)_6(H_2O)_4]^+$	$^{[5]}$Al(OH)$^{[6]}$Al	3763–3803	3740–3745(IIb)
		$^{[5]}$Al-OH	3779–3826	
		$^{[6]}$Al-OH	3795	3785–3800(Ib)
		Al-OH_2	2820–3780	
γ-Al_2O_3 model	$[(H_2O)_3(OH)_2Al(OH)Al(OH)_3]$	$^{[4]}$Al(OH)$^{[6]}$Al	3702	3679
		$^{[4]}$Al-OH	3783–3823	3739(Ia)
		$^{[6]}$Al-OH	3761–3781	3786(Ib)
		Al-OH_2	2845–3754	3000–3700
Terminal Protonation	$[(H_2O)_4(OH)Al(OH)Al(OH)_3]^+$	$^{[4]}$Al(OH)$^{[6]}$Al	3714	3760–3780(IIa)
		$^{[4]}$Al-OH	3779–3801	3760–3780(Ia)
		$^{[6]}$Al-OH	3830	3785–3800(Ib)
		Al-OH_2	2600–3785	
Bridging Deprotonation	$[(H_2O)_3(OH)_2AlOAl(OH)_3]^-$	$^{[4]}$Al-OH	3731–3747	3760–3780(Ia)
		$^{[5]}$Al-OH	3757–3764	3785–3800(Ib)
		Al-OH_2	2507–3694	
Tetrahedral $Al_2(OH)_6$		$^{[4]}$Al(OH)$^{[4]}$Al	3784	
model	$[Al_2(OH)_6]$	$^{[4]}$Al-OH	3863–3865	3760–3780(Ia)
Terminal Deprotonation	$[Al_2O(OH)_5]^-$	$^{[4]}$Al(OH)$^{[4]}$Al	3775–3812	
		$^{[4]}$Al-OH	3742–3808	3760–3780(Ia)
Terminal Protonation	$[Al_2(OH)_5(OH_2)]^+$	$^{[4]}$Al(OH)$^{[4]}$Al	3763–3765	
		$^{[4]}$Al-OH	3780–3948	3760–3780(Ia)
		Al-OH_2	2657–3715	
Bridging Deprotonation	$[Al_2O(OH)_5]^-$	$^{[4]}$Al(OH)$^{[4]}$Al	3756	
		$^{[4]}$Al-OH	3753–3763	3760–3780(Ia)
Bridging Protonation	$[Al_2(OH)_5(OH_2)]^+$	$^{[4]}$Al(OH)$^{[4]}$Al	3720	
		$^{[4]}$Al-OH	3858–3936	3760–3780(Ia)
		Al-OH_2	3447–3541	

Note: Experimental values from Boehm and Knözinger (1983) except for γ-Al_2O_3 from Koretsky et al. (1997). Ia = terminal $^{[4]}$Al-OH, Ib = terminal $^{[6]}$Al-OH, IIa = bridging $^{[4]}$Al(OH)$^{[6]}$Al, and IIb = bridging $^{[6]}$Al(OH)$^{[6]}$Al assignments of Boehm and Knözinger (1983).

bination of this donor and acceptor type of hydrogen bonding found in the Al-(OH) groups could weaken the O-H bond enough to decrease ν(OH) by the 30 cm^{-1} found in these calculations (Kubicki et al. 1993).

Positively charging the gibbsite model cluster via protonation results in increases of calculated ν(OH) for the isolated Al-(OH) groups, so that the model frequency range overlaps the observed values (Table 1). Positively charged clusters, such as that in Figure 4c, represent gibbsite surfaces that have been in contact with solutions with a *pH* less than the PZC of gibbsite (i.e., surfaces with an excess of protons). Measurement of Al-oxyhydroxide surface vibrational frequencies as a function of solution *pH* would be an interesting test of the above two hypotheses. If the latter is correct, ν(OH) for Al-(OH) groups should increase with lower solution *pH* values; and, if the former is correct, ν(OH) for Al-(OH) groups should decrease with lower solution *pH* values due to hydrogen bonding between Al-(OH) and Al-(OH_2) groups.

Protonation of a second terminal Al-(OH) group in the model gibbsite cluster gives a doubly charged molecule with vicinal Al-$(OH_2)^+$ groups (Fig. 4d). The +2 charge on the molecule does not significantly affect the bridging OH frequencies compared to the neutral molecule, but the terminal OH frequencies are raised 40 to 60 cm^{-1} so that they are computed to be slightly above the range found experimentally (Table 1). Hydrogen bonding between all OH groups is reduced in this cluster and the over ν(OH) range is approximately 250 cm^{-1} as compared to ranges of 400 to 1600 cm^{-1} for other clusters.

Although deprotonation of a bridging OH group in the

model gibbsite cluster leads to a coordination change to $^{[5]}$Al (Fig. 3b), we have included a frequency analysis of this fully optimized structure because we cannot preclude this relaxation mechanism as an actual mineral surface reaction. Table 1 shows that the calculated ν(OH) of the bridging OH group decreases to 70 cm^{-1} less than the experimental value (Boehm and Knözinger 1983) in this case. Calculated terminal ν(OH) frequencies can be nearly as high as the observed range (3711–3774 vs. 3785–3800 cm^{-1}), but the lower end of the calculated frequency range is 60 cm^{-1} below this range due to increased hydrogen bonding in the negatively-charged cluster. Infrared spectra of the mineral surface after reaction in solution at a *pH* above the PZC would be useful to check if any of these shifts occur.

γ-Al_2O_3. For the $^{[6]}$Al-$^{[4]}$Al dimer (Fig. 5a), the calculated ν(OH) stretching frequencies for terminal $^{[6]}$Al-OH and $^{[4]}$Al-OH reproduce observed frequencies fairly well (Table 1). However, the bridging (OH) group is predicted to vibrate at a lower frequency, 3702 cm^{-1}, than the assigned band ν(OH) stretch for $^{[4]}$Al-(OH)-$^{[6]}$Al at 3760–3780 cm^{-1} (Boehm and Knözinger 1983). A band near 3700 cm^{-1} has been observed in spectra of γ-Al_2O_3, but this band has been assigned to ν(OH) stretches where the O atom is attached to three $^{[6]}$Al atoms (Boehm and Knözinger 1983). This previous assignment may be in error because $^{[4]}$O is not a common species at low pressure. Instead, the 3700 cm^{-1} band is more likely due to ν(OH) stretches in $^{[4]}$Al(OH)$^{[6]}$Al linkages.

Protonation of one of the terminal $^{[6]}$Al-(OH) groups increases the frequency of the other $^{[6]}$Al-(OH) group by approximately 60 cm^{-1} (Table 1), but otherwise has little effect on other ν(OH) frequencies. In contrast, deprotonating the bridging O decreases the $^{[4]}$Al-OH modes by approximately 60 cm^{-1} with only a 10 cm^{-1} decrease on the $^{[6]}$Al-(OH) frequencies.

Tetrahedral $Al_2(OH)_6$ model. The tetrahedral $Al_2(OH)_6$ cluster (Fig. 6) is a hypothetical construct. Its calculated values were included in Table 1 because ν(OH) frequencies can be correlated with relative acidities (Datka et al. 1988; Gil et al. 1994; Hunger et al. 1996) and the protonation behavior of this type Al-(OH) group is of theoretical interest as will be discussed below.

Proton affinities

Corundum. The proton affinity of a bridging O atom in the corundum model (i.e., the calculated potential energy difference between Figs. 1a and 1e) is 1290 kJ/mol (Table 1). Although this model value is an upper limit because the Al-O-Al configuration is not fully minimized with respect to potential energy, it does fall within the range of 1190 to 1300 kJ/mol determined for bridging O atoms in zeolites (Datka et al. 1988). The model proton affinity of the bridging O in the Al-octahedral cluster is also close to the calculated value of 1301 kJ/mol for an Al-O-Si O where both Al and Si in the Al-O-Si linkages tetrahedrally coordinated (Kubicki et al. 1996). Similarly, the calculated proton affinities of 1402 and 2196 kJ/mol (Table 1) for removing the first and second proton from a terminal Al-(OH_2) group in the corundum model are close to the values of 1317 and 2004 kJ/mol calculated for a tetrahedral Al-(OH_2) group (Kubicki et al. 1995). Absolute accuracy in these types of energy calculations is typically not high, but relative energetics are generally predicted fairly well (Kubicki et al. 1996). Thus, formation of Al-(OH) and Al-(OH_2) groups on α-Al_2O_3 should occur under higher *pH* conditions than their tetrahedral counterparts because removing protons from the terminal O in the corundum model would require 100 to 200 kJ/mol more energy than tetrahedral Al-(OH) and Al-(OH_2) groups. This conclusion is consistent with isoelectric points of $^{[6]}$Al-OH and $^{[4]}$Al-OH as given in Parks (1967).

Gibbsite. Deprotonation of a Al-(OH_2)-Al site in the constrained gibbsite model (Fig. 3c) requires 1041 kJ/mol. However, the Al-(OH_2)-Al structure is not likely to be observed on mineral surfaces, however, because the model calculations predict that this configuration will spontaneously break down to form the defect surface structure shown in Figure 3e.

The deprotonation energy of the Al-(OH)-Al group of Figure 3a, is calculated to be 1640 kJ/mol when the deprotonated cluster is constrained and 1320 kJ/mol if fully relaxed. Thus, if this 320 kJ/mol difference represents a possible range of proton affinities for Al-(OH)-Al sites in gibbsite, deprotonation of this group may occur over a range of *pH* conditions depending on the amount of local structural relaxation permissible surrounding the site. For example, an Al-(OH)-Al linkage on the mineral surface at a corner or edge may fully relax upon deprotonation; whereas, Al-(OH)-Al linkages on a planar surface may be more highly constrained by the surrounding crystal lattice. In this scenario, the corner and edge Al-(OH)-Al groups would deprotonate at lower *pH* than the corresponding sites where the Al atoms were fully bonded to the bulk crystal. If structural relaxation such as this can result in a significant range of proton affinities, then it is possible that a range of pK_a values may exist at different sites on mineral surfaces even in minerals with only one type of surface O. Thus, determinations of surface pK_a's from bulk surface titrations may miss the individual surface deprotonation reactions at the more reactive surface sites.

For the following series of terminal deprotonation reactions,

$$\underset{\text{(Fig. 4d)}}{2\text{Al-}(OH_2)^+} \rightarrow \underset{\text{(Fig. 4c)}}{\text{Al-}(OH_2)^+} + \text{Al-(OH)}$$
$$\rightarrow \underset{\text{(Fig. 4a)}}{2\text{Al-(OH)}} \rightarrow \underset{\text{(Fig. 4b)}}{\text{Al-}O^-} + \text{Al-(OH)}, \quad (5)$$

the proton affinities are 657, 1105, and 1710 kJ/mol, respectively. This range covers the difference between the gas-phase proton affinities of H_3O^+ and H_2O (697 and 1635 kJ/mol; Lias et al. 1988). Gas-phase proton affinities calculated for H_2O and H_3O^+ using the same basis sets are close to the experimental values, so we have reason

TABLE 2. Calculated energy changes for deprotonation of various O sites

Model	Site	ΔE kJ/mol
Corundum II	Al-OH-Al	+68
Gibbsite Terminal	Al-OH	+414†
	$Al\text{-}OH_2^+$	+146
	Vicinal 2[$Al\text{-}OH_2^+$]	+40
Gibbsite Bridging	Al-OH-Al	+83*
$\gamma\text{-}Al_2O_3$ Terminal	$^{[4]}Al\text{-}OH_2^+$	+121*
	$^{[6]}Al\text{-}OH_2$	+47*
	Geminal $^{[6]}Al\text{-}(OH_2)_2^+$	+85
$\gamma\text{-}Al_2O_3$ Bridging	Al-OH-Al	+88*
Tetrahedral $Al(OH)_3$ Terminal	Al-OH	+246
	$Al\text{-}OH_2^+$	−55
Tetrahedral $Al(OH)_3$ Bridging	Al-OH-Al	+118
	$Al\text{-}OH_2^+$-Al	−131

Note: ΔE values from HF/6-311+G** SCIPCM are relative to the protonation of an H_2O molecule in solution [e.g., Al-OH + $H_2O{\cdot}8(H_2O) \rightarrow$ Al-O^- + $H_3O^+{\cdot}8(H_2O)$].

* = Al coordination change.

† = ZPE estimated from $Al_2(OH)_6(H_2O)_4$ value −35 kJ/mol for one OH bond (Fleischer et al. 1993).

to believe our model proton affinities are reasonably accurate. Model calculations predict that the gas-phase reactions

$$\text{Al-(OH)} + H_2O \rightarrow \text{Al-}O^- + H_3O^+ \quad (6a)$$

$$\text{Al-(OH)} + OH^- \rightarrow \text{Al-}O^- + H_2O \quad (6b)$$

favor the reactants by −1013 and −42 kJ/mol, respectively. This is consistent with the pK_{a2} of gibbsite being 7 (pK_{a2} = 8.1; Schindler and Stumm 1987) since formation of hydroxide ion is favored. The reaction

$$\text{Al-}(OH_2)^+ + H_2O \rightarrow \text{Al-(OH)} + H_3O^+ \quad (7)$$

is predicted to require +408 kJ/mol suggesting that Al-$(OH_2)^+$ also forms above *pH* 7. Our model also predicts that the pK_a for the formation of vicinal Al-$(OH_2)^+$ groups should be less than seven because

$$2[\text{Al-}(OH_2)^+] + H_2O \rightarrow \text{Al-}(OH_2)^+ + \text{Al-(OH)} + H_3O^+ \quad (8)$$

is favored by −40 kJ/mol. This is consistent with a pK_{a1} of less than seven for gibbsite (pK_{a1} = −5.2; Schindler and Stumm 1987).

The effects of solvation and entropy must be taken into account before these proton affinities can be translated into ΔG's and pK_a's, but it has been shown previously that such gas-phase proton affinities do correlate closely with aqueous phase pK_a's (Rustad et al. 1996; Kubicki et al. unpublished results). As a test of how solvation would affect our results, we performed self-consistent reaction field calculations (Miertus et al. 1981) on a selected set of molecules. To account for solvation, we chose to use the self-consistent isodensity polarized continuum model (SCIPCM) of Keith and Frisch (1994) as implemented in Gaussian 94 (Frisch et al. 1995).

Table 2 contains values for calculated aqueous-phase deprotonation energies. All the model surface cluster results are added to −1187 kJ/mol, which is the energy calculated for the protonation of a water molecule

$$H_2O{\cdot}8(H_2O) + H^+ \rightarrow H_3O^+{\cdot}8(H_2O) \quad (9)$$

with the SCIPCM calculations at the HF/6-311+G** level. Examination of Table 2 reveals that the deprotonation energies of terminal gibbsite bonds decrease in the order Al-OH > $Al\text{-}OH_2^+$ > Al-(OH)-Al > vicinal $Al\text{-}OH_2^+$, and all four require energy relative to protonation of H_2O (i.e., the values are positive). Thus, protons are predicted to be energetically more stable in vicinal Al-$(OH_2)^+$ sites than in water, which implies that these sites would protonate above *pH* 7. This conclusion is different than that based on the gas-phase calculations discussed above where the same reaction is −40 kJ/mol. The actual value for this reaction probably falls in between these values because the gas-phase calculations neglect solvation effects entirely and the dielectric continuum calculations overestimate solvation effects. There are two reasons for the present dielectric continuum model to overestimate the effect of water. First, the whole cluster has been embedded in the dielectric continuum rather than just the surface groups as would occur at a mineral-water interface. Second, using the value of ϵ for bulk water overestimates the actual value of ϵ at a mineral surface because this parameter can decrease near charged surfaces (Gilson et al. 1993). Future models should include water molecules for explicit solvation and a more realistic value for ϵ near the mineral surface.

$\gamma\text{-}Al_2O_3$. From the cluster $(H_2O)_3(OH)_2Al(OH)Al(OH)_3$, model deprotonation energies were predicted for sites on $\gamma\text{-}Al_2O_3$. Site proton affinities decrease in the order $^{[4]}Al\text{-}OH_2^+$ > Al-(OH)-Al ≈ geminal Al-$(OH_2)_2^+$ > $^{[6]}Al\text{-}OH_2$ both with (Table 2) and without solvation as calculated by SCIPCM. However, except for the geminal $^{[6]}Al\text{-}(OH_2)_2^+$ deprotonation, each of these reactions is complicated by Al coordination changes that accompany removing a proton from a surface OH group. Although full relaxation (e.g., Fig. 5) is not expected on a mineral surface under normal titration conditions, coordination changes are possible on surfaces undergoing dissolution (Bunker et al. 1988). Hence, examination of dissolving mineral surfaces for various Al coordination states is necessary to verify whether these reactions occur. If various coordination states do appear on dissolving aluminum oxide or aluminum hydroxide surfaces, then it becomes very difficult to rationalize dissolution mechanisms in terms of surface titration data on a non-dissolving mineral.

Tetrahedral $Al(OH)_3$ model. Stabilities of the various proton sites on tetrahedral $Al(OH)_3$ sites are distinct from one another. The Al-OH site would form under more basic conditions, followed by the Al-(OH)-Al site (Table 2). Both the $Al\text{-}OH_2^+$ and $Al\text{-}OH_2^+$-Al sites are predicted to be unstable relative to H_3O^+ in water and so would not form except under extremely acidic conditions. Comparison of these tetrahedral aluminum oxide deprotonation energies with those calculated for $^{[4]}Al$ sites in $\gamma\text{-}Al_2O_3$ is

difficult due to the Al coordination changes predicted for the latter model. However, it is worthwhile to compare the tetrahedral $Al(OH)_3$ deprotonation energies with those calculated for Al-OH sites in model feldspar molecules (Kubicki et al. 1996). For instance, gas-phase calculations with the HF/6-311+G** basis set predict proton affinities of +895 and +756 kJ/mol for terminal and bridging O atoms in tetrahedral $Al(OH)_3$; whereas the same methodology results in values of +977 and +953 kJ/mol for terminal Al-$(OH_2)^+$ and Al-(OH)-Si sites in the molecule $Na\{[(OH)_3SiO]_3Al\text{-}OH\}$. In both cases, protonation of the terminal OH group is favored, but the values of the energy changes are significantly different between the model Al-hydroxide and model feldspar sites. Consequently, using aluminum oxide potentiometric data to predict the surface protonation behavior of aluminosilicates (e.g., Parks 1967) could be inaccurate.

Summary

The above discussion of results and implications has been presented with two hypotheses in mind. (1) The structures, infrared frequencies, and proton affinities calculated for these small model molecules are similar to values found experimentally for mineral surfaces. Michalak et al. (1996) have shown that charges, bond orders, and electrostatic potentials depend weakly on cluster size. In combination with the agreement demonstrated between calculated and experimental OH frequencies, the cluster approximation seems a reasonable one to make at this point. On the other hand, long-range electrostatic effects can be important in modeling surfaces (Pacchioni et al. 1997). Although ideally we should model these reactions with a 2-D periodic mineral surface and bulk solution (e.g., Schneider et al. 1998), including the critical aspects of protonation and defect sites has proven problematic. (2) The protonation and deprotonation of surface O atoms is a more complicated process than is generally accounted for in most models to date. Even if the reader is not convinced of our first hypothesis, the second is valid because differences between actual minerals surfaces and our model molecules will only add to the complexity of the situation. We suggest that multi-site models for protonation reactions at mineral surfaces must account for a significant variation in acidities. To quote Schindler and Stumm (1987), ''The possibility of hydroxyl groups covering a continuous spectrum of chemical properties cannot be positively ruled out.'' Studies such as Koretsky et al. (1998) are a good starting point for defining the number of possible sites. Molecular modeling of these sites may help us start to determine the possible range of individual surface acidities.

The results of our calculations have consistently shown that protonation of terminal Al-(OH) groups does not lead to bond weakening that would enhance dissolution of minerals. Protonation of bridging Al-(OH)-Al groups often results in spontaneous bond breaking to lower the energy of these clusters. These two points argue strongly against the surface protonation model for dissolution.

Lastly, the possibility of coordination changes on mineral surfaces that follow corresponding aqueous phase coordination changes must also be considered when addressing dissolution mechanisms (e.g., Bunker et al. 1988; Hellmann et al. 1990). Similar results have been predicted for goethite in calculations using periodic boundary conditions as well (Rustad, personal communication). Thus, it is not likely that the predicted coordination changes are merely an artifact of the cluster approximation. The model results presented here suggest several sets of experiments that would be useful based on vibrational and nuclear magnetic resonance spectroscopy of surfaces at varying *pH*. Changing coordination states on mineral surfaces may be a crucial factor in the adsorption and dissolution behavior of these phases.

Acknowledgments

The comments of Jim Rustad and an anonymous reviewer are gratefully acknowledged. J.D.K. acknowledges the National Research Council Research Associateship program. S.E.A. and J.D.K. acknowledge the financial support of The Office of Naval Technology and The Office of Naval Research. Computer resources were supplied by the DoD High-Performance Computing initiative through the Space and Naval Warfare Systems Center, the Army Corps of Engineers Waterways Experiment Station, and the Aeronautical Systems Center.

References cited

Berner, R.A. and Holdren, G.R. Jr. (1979) Mechanism of feldspar weathering: II. Observations of feldspars from soils. Geochimica et Cosmochimica Acta, 43, 1173–1186.

Berner, R.A., Sjoberg, E.L., Velbel, M.A., and Krom, M.D. (1980) Dissolution of pyroxenes and amphiboles during weathering. Science, 207, 1205–1206.

Bleam, W.F., Welhouse, G.J., and Janowiak, M.A. (1993). The surface Coulomb energy and proton Coulomb potentials of pyrophyllite {010}, {110}, {100}, and {130} edges. Clays and Clay Minerals, 41, 305–316.

Blum, A.E. and Lasaga, A.C. (1991) The role of surface speciation in the dissolution of albite. Geochimica et Cosmochimica Acta, 55, 2193–2201.

Boehm, H.P. (1966) Chemical identification of surface groups. Advances in Catalysis, 12, 179–274.

Boehm, H.P. and Knözinger, H. (1983) Nature and estimation of functional groups on solid surfaces. In J.R. Anderson and M. Bouchart, Eds., Catalysis Science and Technology, pp. 39–207. Springer, New York.

Brady, P.V. and Walther, J.V. (1989) Controls on silicate dissolution rates in neutral and basic pH solutions at 25°C. Geochimica et Cosmochimica Acta, 53, 2823–2830.

Bunker, B.C., Tallant, D.R., Headley, T.J., and Turner, G.L. (1988) The structure of leached sodium borosilicate glass. Physics and Chemistry of Glasses, 29, 106–120.

Burch, T.E., Nagy, K.L., and Lasaga, A.C. (1993) Free energy dependence of albite dissolution kinetics at 80°C and pH 8.8. Chemical Geology, 105, 137–162.

Carroll-Webb, S.A. and Walther, J.V. (1988) A surface complexation model for the pH-dependence of corundum and kaolinite dissolution rates. Geochimica et Cosmochimica Acta, 52, 2609–2623.

Datka, J., Boczar, M., and Rymarowicz, P. (1988). Heterogeneity of OH groups in NaH-ZSM-5 zeolite studied by infrared spectroscopy. Journal of Catalysis, 114, 368–376.

Davis, J.A. and Leckie, J.O. (1978) Effect of adsorbed complexing ligands on trace metal uptake by hydrous oxides. American Chemical Society, 12, 1309–1315.

Dowty, E. (1995) ATOMS for Windows, V 3.1, Shape Software: Kingsport, Tennessee.

Fleischer, U., Kutzelnigg, W., Bleiber, A., and Sauer, J. (1993) ^{1}H NMR

chemical shift and intrinsic acidity of hydroxyl groups. Ab initio calculations on catalytically active sites and gas-phase molecules. Journal of the American Chemical Society, 115, 7833–7838.

Foresman, J.B. and Frisch, A.E. (1993) Exploring Chemistry with Electronic Structure Methods, Gaussian, Inc., Pittsburgh, Pennsylvania. 302 pp.

Frisch, M.J., Trucks, G.W., Schlegel, H.B., Gill, P.M.W., Johnson, B.G., Robb, M.A., Cheeseman, J.R., Keith, R., Petersson, G.A., Montgomery, J.A., Raghavachari, K., Al-Laham, M.A., Zakrzewski, V.G., Ortiz, J.V., Foresman, J.B., Peng, C.Y., Ayala, P.Y., Chen, W., Wong, M.W., Andres, J.L., Replogle, E.S., Gomperts, R., Martin, R.L., Fox, D.J., Binkley, J.S., Defrees, D.J., Baker, J., Stewart, J.P., Head-Gordon, M., Gonzalez, C., and Pople, J.A. (1995) Gaussian 94 Revision B.3. Gaussian, Inc., Pittsburgh, Pennsylvania.

Furrer, G. and Stumm, W. (1986). The coordination chemistry of weathering: I. Dissolution kinetics of δ-Al_2O_3 and BeO. Geochimica et Cosmochimica Acta, 50, 1847–1860.

Gil, B., Broclawik, E., Datka, J., and Klinowski, J. (1994). Acidic hydroxyl groups in zeolites X and Y: A correlation between infrared and solid-state NMR spectra. Journal of Physical Chemistry, 98, 930–933.

Gilson, M.K., Davis, M.E., Luty, B.A., and McCammon, J.A. (1993) Computation of electrostatic forces on solvated molecules using the Poisson-Boltzmann equation. Journal of Physical Chemistry, 97, 3591–3600.

Hellmann, R., Eggleston, C.M., Hochella, M.F., and Crerar, D.A. (1990) The formation of leached layers on albite surfaces during dissolution under hydrothermal conditions. Geochimica et Cosmochimica Acta, 54, 1267–1281.

Hochella, M.F. Jr. and White, A.F. (1990) Mineral-Water Interface Geochemistry. In Mineralogical Society of America Reviews in Mineralogy, 23.

Hochella, M.F. Jr. and Banfield, J.F. (1995) Chemical weathering of silicates in Nature: A microscopic perspective with theoretical considerations. In Mineralogical Society of America Reviews in Mineralogy, 31, 353–406.

Holdren, G.R. Jr. and Berner, R.A. (1979) Mechanism of feldspar weathering: I. Experimental studies. Geochimica et Cosmochimica Acta, 43, 1161–1171.

Hunger, B., Miessner, H., Vonszombathely, M., and Geidel, E. (1996) Heterogeneity of Si-OH-Al groups in HNaY zeolites. Journal of the Chemical Society, Faraday Transactions, 92, 499–504.

Kawakami, H. and Yoshida, S. (1985). Quantum-chemical studies of alumina Journal of the Chemical Society, Faraday Transactions 2, 81, 1117–1127.

Kawakami, H., Yoshida, S., and Yonezawa, T. (1984). A quantum-chemical approach to the generation of solid acidity in composite metal oxides. Journal of the Chemical Society, Faraday Transactions 2, 80, 205–217.

Keith, T.A. and Frisch, M.J. (1994) Inclusion of explicit solvent molecules in a self-consistent reaction field model of solvation. American Chemical Society Symposium Series, 569, 22–35.

Keyes, M.P. and Watters, K.L. (1989). Molecular orbital calculations for surface-bound metal species: Rhodium(I) dicarbonyls on alumina or silica. Journal of Molecular Catalysis, 52, 253–262.

Knezovich, J.P., Harrison, F.L., and Wilhelm, R.G. (1987). The bioavailability of sediment-sorbed organic chemicals: A review. Water, Air, and Soil Pollution, 32, 233–245.

Knözinger, H. and Ratnasamy, P. (1978) Catalytic aluminas: Surface models and characterization of surface sites. Catalysis Reviews-Science and Engineering, 17, 31–70.

Koretsky, C.M., Sverjensky, D.A., Salisbury, J.M., and D'Aria, D.M. (1997) Detection of surface hydroxyl species on quartz, γ-alumina and feldspars using diffuse reflectance infrared spectroscopy. Geochimica et Cosmochimica Acta, 61, 2193–2210.

Koretsky, C.M., Sverjensky, D.A., and Sahai, N. (1998) Surface site types on oxide and silicate minerals based on crystal chemistry: Implications for site densities, multi-site adsorption, surface infrared spectroscopy, and dissolution kinetics. American Journal of Science, 298, 349–438.

Kubicki, J.D. and Sykes, D. (1993) Molecular orbital calculations of vibrations in three-membered aluminosilicate rings. Physics and Chemistry of Minerals, 19, 381–391.

Kubicki, J.D., Sykes, D., and Rossman, G.R. (1993) Calculated trends of OH infrared stretching vibrations with composition and structure in aluminosilicate molecules. Physics and Chemistry of Minerals, 20, 425–432.

Kubicki, J.D., Blake, G.A., and Apitz, S.E. (1995). G2 theory calculations on $[H_3SiO_4]^-$, $[H_4SiO_4]$, $[H_3AlO_4]^{2-}$, $[H_4AlO_4]^-$, and $[H_5AlO_4]$: Basis set and electron correlation effects on molecular structures, atomic charges, infrared spectra, and potential energies. Physics and Chemistry of Minerals, 22, 481–488.

———(1996). Ab initio calculations on Q^3 Si^{4+} and Al^{3+} species: Implications for atomic structure of mineral surfaces. American Mineralogist, 81, 789–799.

———(1997). Molecular orbital calculations for modeling acetate-aluminosilicate adsorption and dissolution reactions. Geochimica et Cosmochimica Acta. 61, 1031–1046.

Lasaga, A.C. (1981) Rate laws of chemical reactions. In Mineralogical Society of America Reviews in Mineralogy, 8, 1–68.

Lias, S., Bartmess, J.E., Liebman, J.F., Holmes, J.L., Levine, R.D., and Mallard, W.G. (1988) Journal of Physical Chemistry Reference Data, 17, Supplement 1.

Michalak, A., Hermann, K., and Witko, M. (1996) Reactive oxygen sites at MoO_3 surfaces: ab initio cluster model studies. Surface Science, 366, 323–336.

Miertus, S., Scrocco, E., and Tomasi, J. (1981) Electrostatic interaction of a solute with a continuum. A direct utilization of ab initio molecular potentials for the prevision of solvent effects. Chemical Physics, 55, 117–129.

Morterra, C., Ghiotti, G., Garrone, E., and Boccuzzi, F. (1976) Infrared spectroscopic characterization of the α-alumina surface. Journal of the Chemical Society, Faraday Transactions, 72, 2722–2734.

Nakamoto, K., Marghoshesm, M., and Rundlem, R.E. (1955) Stretching frequencies as a function of distances in hydrogen bonds. Journal of the American Chemical Society, 77, 6480–6488.

Novak, A. (1974) Hydrogen bonding in solids. In J.D. Dunitz, P. Hemmerich, R.H. Holm, J.A. Ibers, C.K. Jorgensen, J.B. Neilands, D. Reinene, and R.J.P. Williams, Eds., Structure and Bonding 18: Large Molecules, 177–216. Springer, New York.

Oxburgh, R., Drever, J.I., and Sun, Y.T. (1994) Mechanism of plagioclase dissolution in acid solution at 25°C. Geochimica et Cosmochimica Acta, 58, 661–669.

Pacchioni, G., Ferrari, A.M., Márquez, A.M., and Illas, F. (1997) Importance of Madelung potential in quantum chemical modeling of ionic surfaces. Journal of Computational Chemistry, 18, 617–628.

Parks, G.A. (1967) Aqueous surface chemistry of oxides and complex oxide minerals. Isoelectric point and zero point of charge. In W. Stumm, Ed., American Chemical Society Advances in Chemistry Series, 67, 121–160.

Paterson, M.S. (1982) The determination of hydroxyl by infrared adsorption in quartz, silicate glasses and similar materials. Bulletin de Mineralogie, 105, 20–29.

Pople, J.A., Schlegel, H.B., Krishnan, R., Defrees, D.J., Binkley, J.S., Frisch, M.J., Whiteside, R.A., Hout, R.F., and Hehre, W.J. (1981) Molecular-orbital studies of vibrational frequencies. International Journal of Quantum Chemistry: Quantum Chemical Symposium, 15, 269–278.

Rebhun, M., Kalabo, R., Grossman, L., Manka, J., and Rav-Acha, C. (1992). Sorption of organics on clay and synthetic humic-clay complexes simulating aquifer processes. Water Research, 26, 79–84.

Rustad, J.R., Felmy, A.R., and Hay, B.P. (1995) Molecular statics calculations of proton binding to goethite surfaces. A new approach to estimation of stability constants for multisite surface complexation models. Geochimica et Cosmochimica Acta, 60, 1563–1576.

Saalfeld, H. and Wedde, M. (1974) Refinement of the crystal structure of gibbsite, Z. Kristallogr., Kristallgeom., Kristallphys., Kristallchem, 139, 129–135.

Schindler, P.W. and Stumm, W. (1987). The surface chemistry of oxides, hydroxides, and oxide minerals. In W. Stumm, Ed., Aquatic Surface Chemistry: Chemical Processes at the Mineral-Water Interface, 83–110.

Schneider, W.F., Hass, K.C., Curioni, A. and Andreoni, W. (1998) Struc-

tural and dynamic investigation of the water/α-alumina interface. Abstracts of Papers of the American Chemical Society, 215, PH45-407.
Shannon, R.D. and Prewitt, C.T. (1969) Effective ionic radii in oxides and fluorides. Acta Crystallographica, B25, 925–946.
Stillings, L.L. and Brantley, S.L. (1995) Feldspar dissolution at 25°C and pH 3: Reaction stoichiometry and the effect of cations. Geochimica et Cosmochimica Acta, 59, 1483–1496.
Stumm, W. and Morgan, J.J. (1981) Aquatic Chemistry, 780 p. Wiley, New York.
Sverjensky, D.A. and Sahai, N. (1996) Theoretical prediction of single site surface protonation equilibrium constants for oxides and silicates in water. Geochimica et Cosmochimica Acta, 60, 3773–3797.
Sykes, D. and Kubicki, J.D. (1996) Four-membered rings in silica and aluminosilicate glasses. American Mineralogist, 81, 265–272.
Sykes, D., Kubicki, J.D., and Farrar, T.C. (1997) Molecular orbital calculation of ^{27}Al and ^{29}Si NMR parameters in Q^3 and Q^4 aluminosilicate molecules and implications for the interpretation of hydrous aluminosilicate glass NMR spectra. Journal of Physical Chemistry. 101, 2715–2722.
Tsyganenko, A.A. and Filimonov, V.N. (1973). Infrared spectra of surface hydroxyl groups and crystalline structure of oxides. Journal of Molecular Structure, 19, 579–589.
Van Cappellen, P. and Qiu, L. (1995) Reactive surface area control on the dissolution kinetics of biogenic silica. Abstracts of the American Chemical Society, 209, 64–GEOC.
Wieland, E., Werhli, B., and Stumm, W. (1988) The coordination chemistry of weathering: III. A potential generalization on dissolution rates of minerals. Geochimica et Cosmochimica Acta, 52, 1969–1981.
Wong, M.W., Wiberg, K.B., and Frisch, M.J. (1995) Ab initio calculation of molar volumes: Comparison with experiment and use in solvation models. Journal of Computational Chemistry, 16, 385–394.
Wyckoff, R.W.G. (1978) Crystal Structures. Interscience Publishers, New York.

Manuscript received December 17, 1997
Manuscript accepted April 29, 1998
Paper handled by Lars Stixrude